Search for the $2S$-$2P$ energy difference in muonic ^{4}He ions

P. Hauser, H. P. von Arb,* A. Biancchetti, H. Hofer, F. Kottmann, Ch. Lüchinger,†
R. Schaeren, F. Studer,* and J. Unternährer‡
Institut für Hochenergiephysik, Eidgenössische Technische Hochschule–Hönggerberg, CH-8093 Zürich, Switzerland
(Received 23 March 1992)

We searched for laser-induced $2S_{1/2}$-$2P_{3/2}$ transitions in $(\mu^- {}^4\mathrm{He})^+$ ions at low pressure (4.1 kPa), where we determined a $2S$ lifetime of 1.014 ± 0.121 μs from the simultaneously measured $2S\rightarrow1S$ two-photon transitions. In contrast to a similar experiment in He gas of 40 bar (4×10^6 Pa) reported by Carboni *et al.* [Nucl. Phys. **A278**, 381 (1977)], which was based on the questionable metastability of the $2S$ state at that pressure, we found no resonance effect at the wavelength $\lambda=811.7$ nm. We can reject this wavelength with a confidence level of less than 2×10^{-3}, and the interval $811.4\leq\lambda\leq812.0$ nm with a greater than 95% probability.

PACS number(s): 36.10.Dr, 12.20.Fv, 42.50.Wm

I. INTRODUCTION

The measurement of the Lamb shift, i.e., the $2S$-$2P$ energy difference, in the lightest muonic atoms leads to precise tests of the vacuum polarization and to the determination of the nuclear charge radii [1]. In contrast to the electronic H atom, vacuum polarization and finite nuclear size are the main contributions to the $2S$-$2P$ energy difference in muonic atoms. The contributions of nuclear polarization and vertex corrections are small [2]. For $Z\leq2$ the vacuum polarization exceeds the finite-size contribution by an order of magnitude and electron screening effects are absent. A good experimental precision can be attained by using laser resonance techniques. For muonic He (μHe) the wavelength corresponding to the $2S$-$2P$ energy difference is around 0.8 μm and the relative natural linewidth is only about 1000 ppm.

In the 1970s the $2S$-$2P$ energy difference in muonic helium ions $(\mu^- {}^4\mathrm{He})^+$ was measured at CERN [3,4]. That experiment was based on the following principles: The transition from the metastable $2S$ state to the $2P$ state was induced by intense laser light (resonance absorption), and the $K\alpha$ x ray emitted during the immediately following $2P$-$1S$ transition ($\tau_{2P}=5\times10^{-13}$ s) was detected. The laser pulse had to be delayed relative to the muon stop signal, in order that the laser-induced $K\alpha$ x rays could be separated from the prompt ones of the muonic cascade. This required a sufficiently long $2S$ lifetime (~1 μs) and a $2S$-state population probability of a few percent.

The Lamb-shift experiment at CERN was performed at a He pressure of 40 bar. In previous measurements [5,6] the $2S$ lifetime had been determined at pressures between 7 and 50 bar, and only small deviations from the lifetime in vacuum (no collisions) $\tau_{2S}^0=1.75$ μs were found. There was, however, a contradiction between theoretical predictions [7–9] of high radiative collisional $2S$-quenching rates and the absence of the corresponding $2P$-$1S$ transitions in the experimental data.

We investigated the $(\mu^- {}^4\mathrm{He})_{2S}$ lifetime in the pressure region between 65 mbar and 6 bar [10,11]. At 6 bar no delayed x rays from $2S$ decays were found, which suggested an upper limit $\tau_{2S}<150$ ns. Below 1 bar delayed x rays were measured and τ_{2S} was determined as a function of pressure. Based on these measurements a model for the pressure dependence of the quenching rates was established, which confirmed the predicted formation of $\{\mathrm{He}\text{-}\mu\mathrm{He}\}^+$ molecular ions [12] and fixed experimentally their formation rate.

The absence of a satisfying theoretical explanation for long lived $(\mu\mathrm{He})_{2S}$ at high density [12–15] led to two more recent measurements in the pressure region of 40 bar, one establishing an upper limit of the $(\mu\mathrm{He})_{2S}$ lifetime $\tau_{2S}<47$ ns [16] and the other excluding the presence of metastable $(\mu\mathrm{He})_{2S}$ states [17]. This situation strongly suggested the measurement of the $2S$-$2P$ energy difference in muonic helium at low pressure, where the $2S$ lifetime is long (≥1 μs) according to experimental data [10,11], which are in qualitative as well as quantitative agreement with theoretical calculations.

In the present experiment the He pressure was 4.1 kPa=41 mbar (at $T=300$ K), corresponding to a density $\rho=6.6\times10^{-6}$ g/cm^3. At this pressure the relative population of the $2S$ level can be determined from the measured K-line intensity ratios and amounts to $\epsilon_{2S}=(2.6\pm0.3)\%$ [11]. The goal of the experiment was to check the $2S_{1/2}$-$2P_{3/2}$ resonance wavelength $\lambda=811.68\pm0.15$ nm as found by Carboni *et al.* [3] at a He pressure of 40 bar, which was in agreement with the predicted value $\lambda^{\mathrm{th}}=812.2\pm1.5$ nm [2] corresponding to a Lamb shift of 1526.5 ± 2.8 meV. This energy difference is the sum of the contributions from vacuum polarization (1678.2 meV), finite nuclear size (-289.6 ± 2.7 meV [18]), vertex and recoil corrections (-10.9 meV), nuclear polarizability (3.1 ± 0.6 meV), and fine structure (145.7 meV). The main uncertainty of the calculated energy splitting results from the experimentally determined rms charge radius of the ^{4}He nucleus (extrapolation of electron-scattering data to small-momentum transfer [18]).

Simultaneously to the laser resonance measurement, we determined the $2S$ lifetime τ_{2S} by detecting both x rays from the $2S \rightarrow 1S$ two-photon decay in coincidence. The calculated two-photon transition rate is $\lambda_{xx} = 1.18 \times 10^5\ s^{-1}$ [19].

II. APPARATUS AND EXPERIMENTAL METHOD

A. Principle of the experiment

The principle of the experiment was to produce $(\mu\text{He})^+_{2S}$ atoms, and to inject a short laser pulse into the muon-stop region within the $2S$ lifetime, i.e., about 1 μs after the formation of the atom. The detection of a μHe-$K\alpha$ x ray in coincidence with the laser pulse then indicated that the laser wavelength corresponded to the $2S$-$2P$ energy difference. Since there was no unique signature for the formation of $2S$ states, the detection of a muon stopping in the helium gas had to be taken as laser trigger, and since only a small fraction ϵ_{2S} of all stopped muons form a μHe $2S$ state, the probability of finding that state at the time of the laser pulse was small.

The main components of the apparatus were a device for trapping muons at a sufficient rate in He gas at a density $\rho \sim 6.6 \times 10^{-6}$ g/cm^3, a muon-stop detector, two x-ray detectors for measuring the radiative transitions in μHe, a tunable laser system to generate a short intense laser pulse at the right wavelength, and a mirror cavity placed in the muon-stop region with optical diagnostic elements. The requirement to synchronize the laser pulse with the muon-stop trigger occurring at random times was a crucial specification for both the laser system and the stop detector. A dye laser pumped by a Q-switched Nd:YAG laser was used. The Nd:YAG laser, running at a repetition rate of 22 pulses per second, was kept each time at a constant inversion level during 1 ms by means of flash lamps. Within this period, the laser pulse could be generated 300 ns after the trigger signal. In order to have a high probability for an occurrence of a trigger signal within the 1-ms-long inversion interval, the average trigger rate for muon stops had to be at least 1000 s^{-1}. Such a high muon-stop rate at low He gas density could only be attained with the "muon bottle" [20] developed at PSI (Paul Scherrer Institut, formerly SIN, Villigen, Switzerland).

B. Muon bottle

The muon bottle and other components of the apparatus are shown in Fig. 1. Negative pions, detected by a multiwire proportional chamber (DLK), were injected axially into a cylindrically symmetric magnetic bottle, where a fraction of them decayed and produced low-energy muons which were trapped by the magnetic field in helical orbits near the axis. The muons were slowed down by collisions with the gas and finally got captured by a He atom. By choosing the "magic momentum" $p_\pi = 39.3$ MeV/c for the incoming pions, the square-shaped energy spectrum of the muons could be made to just include zero energies corresponding to backward decays. Muons with momentum angle $> 55°$ relative to the bottle axis were reflected at the bottlenecks by radial field components and thus experienced an infinitely long gas target. Momentum collimators (Fig. 2) limited the rotation radii and hence the initial energy of stopping muons to ≤ 1 MeV in order to keep the average slowing down

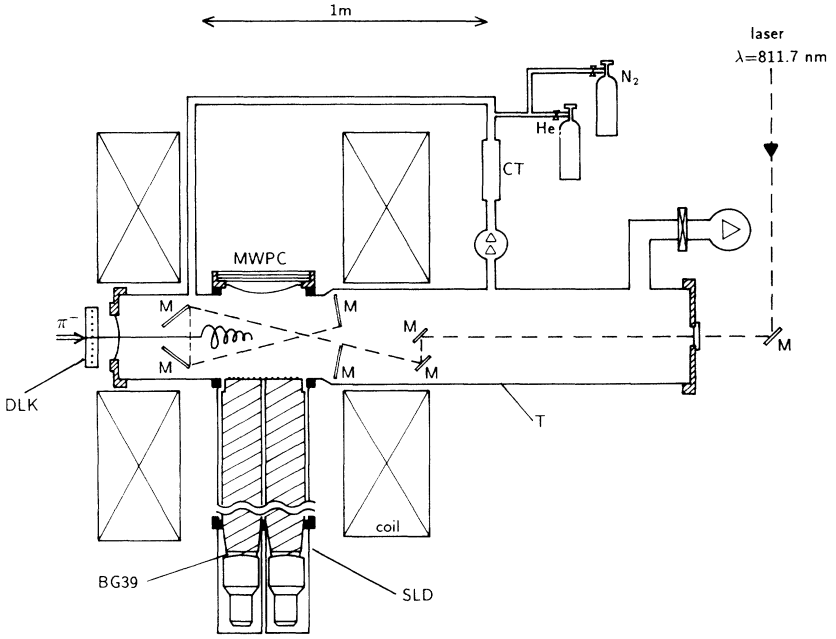

FIG. 1. Schematic of the muon bottle. T, stainless-steel tank filled with the low-pressure He gas; DLK, entrance detector; SLD, scintillation-light detector (wavelength shifter, lucite light guide, filter BG39, and RCA 8854 photomultiplier); MWPC, multiwire proportional chamber (x-ray detector); M, mirror; CT, cold trap.

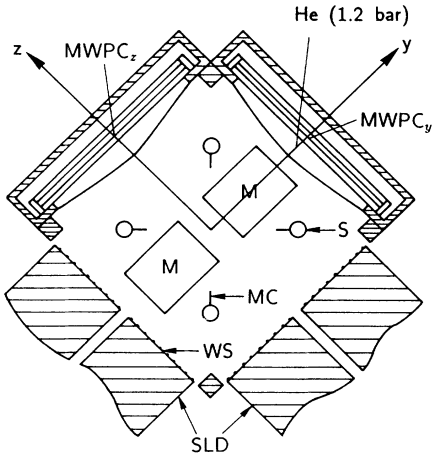

FIG. 2. Cross section of the muon-stop region. SLD, scintillation-light detector; MWPC, multiwire proportional chamber; WS, wavelength shifter; MC, momentum collimator; S, precision support for cavity mirrors; M, cavity mirror.

time as short as possible (~ 0.4 μs). The magnetic field strength was 0.9 T at the center between the coils and 1.4 T within the bottlenecks. The dimensions of the magnets were chosen such that a considerable fraction of the pions (decay length 2.2 m) decayed inside the bottle, i.e., between the two points of maximum field separated by 90 cm. The cross section of the π beam, together with the dimension of the momentum collimators, resulted in a $40\times6\times6$ cm^3 muon-stop volume, which required a high-power laser system and large-area x-ray detectors. The useful stop volume was axially defined by the geometrical acceptance of the stop and x-ray detectors.

The pions were obtained from the 590-MeV proton accelerator of PSI at the $\pi E3$ beam line. Their momentum was $p=40$ MeV/c with a width $\Delta p/p=17\%$ full width at half maximum (FWHM). From a 200-μA proton beam resulted a pion rate of 4.2×10^5 s^{-1} with an additional $5\%\mu^-$ and $3\%e^-$ "contamination." The probability for a pion to decay in the bottle, and the requirements for momentum angle and initial muon energy, lead to a calculated muon-stop probability of $\approx 5.7\times10^{-3}$ per incoming pion, and thus to $\approx$2400 muon stops per second.

C. Stop detector

While muons were slowing down, target-gas atoms were excited or ionized and emitted scintillation light. The fast uv component of the scintillation light was detected by a stop detector, consisting of eight 98-cm-long lucite light guides and eight photomultipliers (Fig. 1). A coating of sodium salicylate on the front faces of the light guides served as wavelength shifter from the uv region to about 420 nm. BG39 filters, which are transparent at 420 nm and absorb wavelengths longer than 800 nm, were used to protect the photomultipliers from laser light scattered in the bottle. In order to increase the scintillation capacity of the target gas, 0.2% N_2 was added to the He gas, raising the scintillation light by a factor of 4 [21]. The light emission in the He-N_2 gas mixture was delayed up to 2 μs. Since pions, and muons from forward decays, give only a small amount of scintillation light compared with stopping muons, the stop detector was sensitive to muons stopping in the gas target. Depending on the initial muon energy, 1–15 photons were measured when a muon was stopped, in agreement with a detector efficiency of 3×10^{-3} and a measured production of one scintillation photon per 300-eV energy loss.

Since the initial energy of stopping muons was spread over an energy range between 0 and 1 MeV, the muons needed different times for slowing down. As a consequence of the moderate statistics of detected scintillation photons, the correlation between the slowing-down time and the number of detected photons was poor. The time of the muon stop could therefore not directly be determined from counting scintillation photons, although it could be limited to an interval of 1.1 μs after the measured pion entrance. Nevertheless, a good trigger for the laser could still be obtained: A fast trigger logic chose those π signals that are followed by a certain number of scintillation photons. The following "stop-light" condition was found to optimize the trigger quality (i.e., the probability that the trigger signal corresponds to a muon stop) and the trigger rate. At least one photon had to be detected within 450 ns and at least four photons within 900 ns relative to an incoming pion ("$\pi S4$ condition"). Clearly, the trigger decision had to be made within the 2S-state lifetime. With the $\pi S4$ condition a trigger quality $Q\approx0.55$ and a trigger rate of 1500 s^{-1} were attained. About $\frac{1}{3}$ of the stopping muons led to a $\pi S4$ trigger.

D. Gas system

As target gas we used high-purity helium with about 0.2% N_2 at a pressure of 4.1 ± 0.1 kPa. The N_2 concentration was periodically checked with a mass spectrometer, which was calibrated with a standard (He+0.2% N_2) gas mixture. The N_2 concentration was found to be $(0.22\pm0.02)\%$ during the whole experiment. The target gas was circulated three times per minute by an oil-free Root's pump through a trap filled with a molecular sieve and cooled by liquid N_2, in order to freeze contaminations such as H_2O and C_nH_m out of the target gas.

A high gas purity was needed to avoid possible μHe-2S quenching. High quenching rates were expected for the highly polarized H_2O molecule [11]. From the measured out-gassing rates and the known gas circulation rate the impurity contamination was estimated. Assuming that H_2O contributes 75% to the impurity contamination, a H_2O partial pressure $(4\pm2)\times10^{-2}$ Pa was determined. The 2S-quenching rates are discussed at the beginning and end of Sec. III.

E. X-ray detectors

For the x-ray detection (see Fig. 2) two flat multiwire proportional chambers (MWPC's) working at a gas pressure of 1.2 bar (1.2×10^5 Pa) were used. The gas mixture consisted mainly of xenon, which has a high absorption efficiency for μHe $K\alpha$ x rays (8.2 keV). The anode plane was formed by wires of 30-μm diameter and 3-mm spac-

ing. Two cathode planes, called the "anterior" and the "posterior" cathodes, were attached symmetrically to the anode at a potential difference of 2.75 kV and defined two 5-mm drift gaps. The signals were read out from the anode wires and contained both timing and energy information. The time resolution of this type of detector was limited by the electron drift time from a cathode to the anode. Since the electron drift velocity in xenon is low, we had to add 15% CO_2 and 5% N_2 to attain a time resolution of 98 ns (FWHM). The time spectrum for 8-keV x rays is shown in Fig. 3. The energy resolution for homogeneous irradiation of the entire 26×26 cm^2 sensitive area was 20% (FWHM) for 8-keV x rays. For other energies it scaled as $E^{-1/2}$.

In order to also detect the μHe $L\alpha$ line at 1.52 keV, which has a short absorption length, thin foils had to be used as windows. Thus a 5-μm aluminized Mylar foil served as anterior cathode. A "prechamber" placed between the anterior cathode and the target gas was flushed with pure helium gas and kept at a pressure slightly below that of the MWPC. The pressure difference of 0.15 mbar pushed the cathode foil smoothly against a thin, precisely positioned wire grid. The main pressure difference of almost 1.2 bar between the prechamber and the target gas was sustained by a 8-μm Mylar foil, supported by a strong stainless-steel grid shaped as a spherical calotte. The prechamber also prevented the diffusion of xenon into the target gas. To avoid background signals caused by charged particles or x rays absorbed in the posterior cathode or the chamber wall behind it, this cathode plane was made almost transparent (wires of 50 μm diameter and 1 mm spacing), and an additional "rejection field plane" was inserted 5 mm behind the cathode and kept at a potential 600 V higher than the cathode.

The detection efficiency, i.e., the product of solid-angle acceptance and absorption efficiency, including the losses caused by absorption in the mylar foils and the supporting grids, was calculated to be 8.6% for $K\alpha$ (8.22 keV) and 2.4% for $L\alpha$ (1.52 keV).

An analysis of the pulse shape, carried out on-line, helped to separate the signals of x rays from those of charged particles. A more detailed description of this detector is given in Ref. [22].

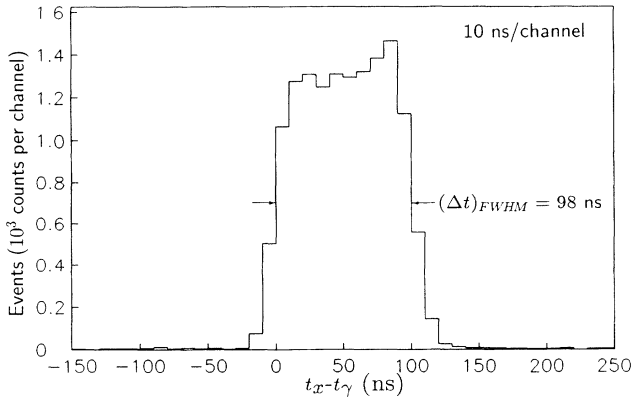

FIG. 3. Time resolution of the x-ray detectors for 8-keV x rays measured with a ^{65}Zn source emitting an 8-keV x ray in coincidence with a highly energetic γ (used as start signal).

F. Laser system

The laser system is shown in Fig. 4. The Nd:YAG and the Styryl-9 dye laser each consisted of an oscillator and several amplifier stages. This laser system was developed at PSI, because available commercial systems could not satisfy the simultaneous requirements for energy, repetition rate, and synchronization. A detailed discussion is given in Refs. [23] and [24]. As explained in Sec. II A, for the synchronization of the laser to the $\pi S4$ trigger, the Nd:YAG laser had to be kept at a constant inversion during a time $T_i = 1$ ms. This was achieved by suitably shaping the current through the flash lamps. The maximum possible repetition rate of the laser was limited by the stress-induced optical effects caused by thermal load of the Nd:YAG crystals. By using crystals in slab geometry instead of cylindrical ones the repetition rate of the Nd:YAG laser could be increased from 6 s to 22 s^{-1} [23].

When a muon-stop trigger fell into the interval of constant inversion, the Nd:YAG oscillator was Q-switched with a Pockels cell and emitted a pulse with an energy of 8 mJ and a duration of 14 ns (TEM_{00}, single axial mode). Two additional slab laser heads acted as preamplifiers. The phase space of the laser beam was cleaned up in a spatial filter before it reached the two final amplifiers, which together delivered an energy of 920 ± 30 mJ per pulse. These pulses were subsequently converted to the second harmonic, i.e., the laser wavelength of 1064 nm was converted to 532 nm. This step was necessary to obtain a wavelength that could be used to pump the dye laser. For high-efficiency frequency doubling two KD*P crystals in series were used with a harmonic beam splitter between them to separate the second harmonic from the fundamental wavelength. With this technique a total energy of 525 ± 25 mJ at 532 nm was attained.

For the oscillator and all amplifiers of the dye-laser system, cells with a cylindrical volume, illuminated by the 532-nm pump beam from four sides, were used [25]. The wavelength of the dye oscillator could be tuned with a diffraction grating in the range between 800 and 850 nm. A set of four prisms in front of the grating, acting as polarizer and beam expander, improved the spectral resolution. Due to the low optical gain in Styryl-9, as many as six amplifier cells were necessary to enhance the oscillator output energy by two orders of magnitude. The delays of the various pump pulses relative to the dye laser were properly adjusted. Telescopes consisting of lens-pinhole-lens combinations, also acting as spatial filters (SPF in Fig. 4), were used to adjust the beam diameter. Polarizers (not shown) along the amplifier chain served to preserve the polarization of the beam. The fraction of the beam leaking through a high-reflection mirror was collected in an optical fiber and guided to a McPherson 1-m monochromator to monitor the wavelength, the linewidth, and the intensity of the amplified spontaneous-emission (ASE) background. A cw krypton calibra-

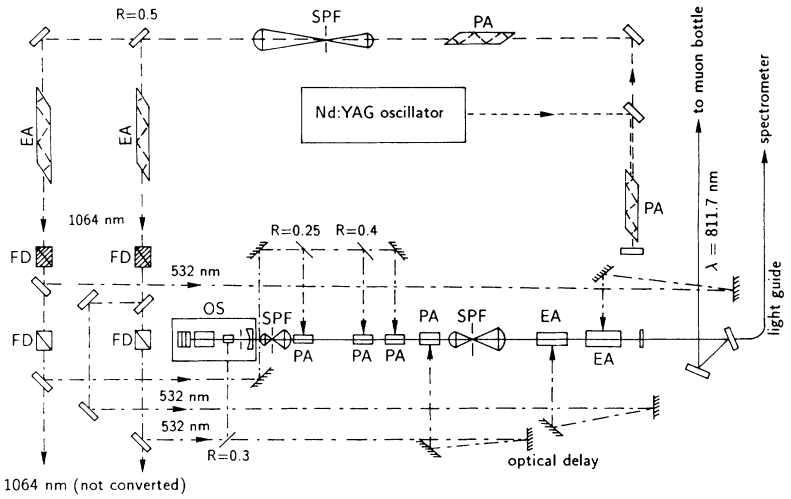

FIG. 4. Laser system consisting of a dye laser pumped by a Nd:YAG laser. OS, oscillator; PA, laser light preamplifier; EA, laser-light end amplifier; SPF, spatial filter; FD, frequency doubler (KD*P crystal). (Not shown: lenses, prism beam expanders, Pockels cells, polarizers, $\lambda/2$ and $\lambda/4$ plates.) Details are given in Refs. [23,24,26].

tion lamp with lines at 810.44 and 811.29 nm (in air) was simultaneously focused into the spectrometer for the absolute calibration. The complete spectral information for each pulse was read out with a diode array at the position of the exit slit of the spectrometer. Figure 5 shows the spectrum for one event. During the experiment the wavelength was 811.70±0.05 nm (in air) with a measured linewidth $(\Delta\lambda)_{\mathrm{FWHM}} \leq 0.07$ nm. The energy was 50–85 mJ per pulse, with a width of 10 ns, and a total relative contribution from ASE of less than 5×10^{-3}. The laser beam was two-times diffraction limited and more than 96% polarized.

G. Optical cavity and diagnostics

The optical components of the laser system were housed in a dust-free hut near the $\pi E3$ area. From there the beam was led with steering mirrors into the muon

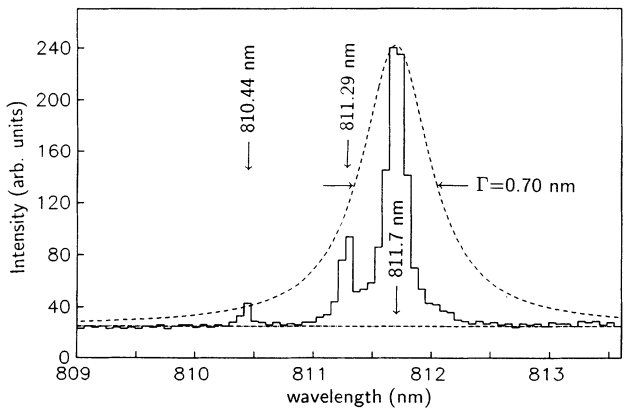

FIG. 5. Typical spectrometer readout with laser line, krypton calibration lines, and natural linewidth Γ of the μHe $2S_{1/2}$-$2P_{3/2}$ transition. All wavelengths λ are measured in air.

bottle. To enhance the $2S$-$2P$ transition probability, the laser light was reflected between a set of mirrors (cavity) crossing the muon-stop volume as many times as possible. To prevent local saturation of the transition probability, a homogeneous intensity distribution in the muon-stop volume was desired. In addition, the duration of illumination should be comparable to the time resolution of the x-ray detectors to minimize the time window for x-ray background. The cavity mirrors had therefore to be placed as close to each other as possible but outside of the muon-stop region and the pion beam to avoid additional x-ray background.

The best solution for these requirements was attained with the four-mirror cavity shown in Fig. 6. Before entering the target vessel the dye-laser beam was magnified by a factor of 10 perpendicular to the cavity mirror plane and then traced horizontally between the four mirrors. In the horizontal direction the laser beam was kept small to avoid injection losses at the cavity entrance. Considering one mirror, the point of incidence of the laser pulse shifted from one mirror edge in decreasing steps towards the opposite edge, then bounced back, and the laser beam left the cavity almost at the entering point. Thus $N \approx 30$ round trips, corresponding to approximately 120 crossings through the muon stop volume, were attained. High-quality mirrors with dielectric coatings (flatness $\lambda/4$, reflectivity=(99.92±0.03)%, transmission=0.05%) were used, resulting in a reduction of power of only 14% after 30 round trips. Before installing the cavity, the mirrors were adjusted manually and afterwards by piezoelectric translators regulated from outside.

To determine the $2S$-$2P$-transition probability, the spatial and temporal distribution of the laser light intensity in the cavity had to be known. The reflection pattern on the mirrors was a two-dimensional projection of the intensity distribution between the mirrors. The small portion of incident light which was transmitted through the mirrors could be used to monitor the intensity distribu-

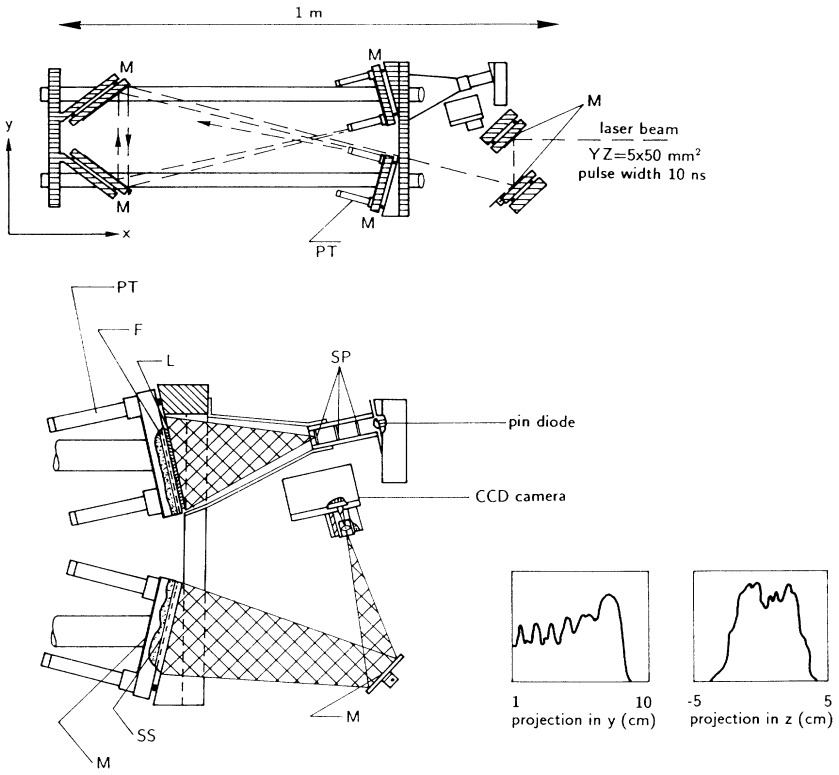

FIG. 6. Laser-beam trace between the four cavity mirrors and monitoring elements in the cavity. M, mirror; PT, piezoelectric translator; F, correction foil; L, Fresnel lens; SP, scatter plates; SS, scattering screen. The projections of a typical two-dimensional camera picture are also shown.

tion (local nonuniformity of the mirror transmission, 2%). Information about the spatial distribution was obtained with a charge-coupled-device (CCD) camera that monitored the light scattered from a screen placed behind one of the mirrors (Fig. 6). The temporal evolution was measured at another mirror by focusing the transmitted light onto a pin diode. A stack of scatter plates in front of the diode made the configuration insensitive to any slight misalignment because the small sensitive area of the pin diode sampled a representative average over the whole intensity distribution. The nonuniform imaging properties of the Fresnel lens used for the focusing (low f number) were compensated for with a suitable attenuation foil. Fine adjustment of the mirror cavity could easily be performed by maximizing the pulse height and pulse width of the pin diode. The pulse width was typically 270 ns. From this pulse width and the known cavity round-trip time (8.8 ns) the number of round trips mentioned above is obtained. During the experiment the information of the diode was recorded for each event with a 100-MHz flash amplitude-to-digital converter (FADC) (Fig. 7). The increase of the signal in the first 100 ns was caused by a residual dependence of the diode output on the beam position. This effect had been studied separately and is well understood [23]. The calibration of the integral of the diode (in terms of energy) was obtained by measuring periodically the laser energy at the entrance to the muon bottle with a calibrated energy meter, and by detailed investigations after the experiment, when the cavity was accessible and thus all possible laser intensity losses at the injection in the cavity, etc., could be analyzed. The injection losses were small ($<2\%$). The error of energy monitoring amounted to $\pm 7.5\%$, resulting mainly from the uncertainty of the calibration of the energy meter ($\pm 5\%$) and from the uncertainty of the cavity losses ($\pm 4.5\%$).

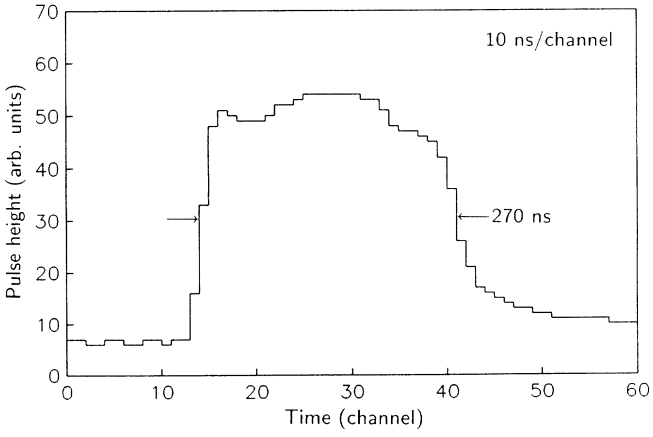

FIG. 7. Pulse shape of the pin diode (in the cavity) for a typical event, digitized by a 100-MHz FADC.

H. Electronics and data acquisition

Three event types were recorded by the data acquisition electronics.

(i) *SXL events,* which were characterized by the detection of an x ray that fell into a gate started by a pion, with the $\pi S4$ trigger condition satisfied and the laser fired.

(ii) *SX events,* which had a signature similar to the SXL events, except that the laser was not fired and only x rays delayed relative to the muon stop were accepted (to prevent filling the magnetic tapes with uninteresting data). In the delayed-time region about nine times more SX events than SXL events were recorded to obtain good statistics for the determination of the background.

(iii) *XX events,* which were characterized by the detection of two x rays, i.e., one in each detector, with a mutual time difference ≤ 500 ns.

A simplified scheme of the electronic logic is shown in Fig. 8. Three types of gates (1XL, 1X, XX) determined the time during which the corresponding events were accepted. Their timing sequence is shown at the top of Fig. 8. Each time the Nd:YAG laser reached the inversion level, a 1-ms *"1XL gate"* was started. If a $\pi S4$ trigger fell in this gate, the laser was fired with a fixed delay relative to the pion entrance time. The 1XL gate was followed by nine consecutive *"1X gates,"* each with the same width. After the last 1X gate the *"XX gate"* started. It ended

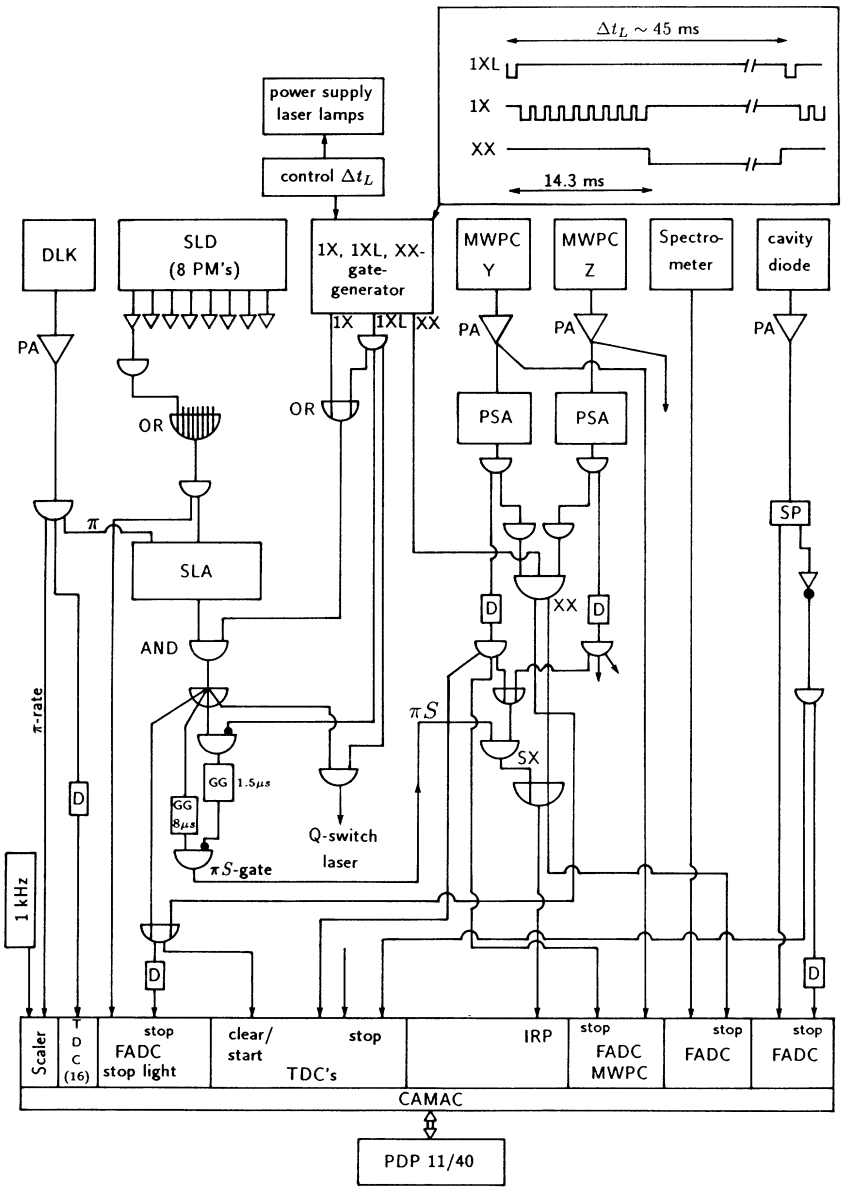

FIG. 8. Block diagram of the electronics. PA, preamplifier; SLD, scintillation light detector; PSA, pulse-shape analyzer; SLA, scintillation-light analyzer; D, delay; GG, gate generator; SP, passive split; FADC, flash amplitude-to-digital converter; TDC, time-to-digital converter.

with the start of the next 1XL gate. An average laser repetition rate of 22 s^{-1} resulted in an XX-gate width of 31 ms.

The signals of the eight photomultipliers of the stop detector were individually amplified and fed to discriminators sensitive to one-photon pulses. The logical "OR" (superposition) of these eight channels was passed on to the "scintillation-light analyzer" (SLA) and to a FADC (Le Croy WFA 2256) which digitalized and stored the train of pulses. The pulse train from the preamplifier of the pion entrance detector (DLK) was discerned with a pulse width of 200 ns, creating a fixed electronical dead time. These digitized pulses started the SLA and were recorded by 16 computer aided measurement-and-control (CAMAC) time-to-digital converters (TDC's) after a 9-μs delay. The 9-μs delay allowed the registration of the prehistory of each event. The 16 CAMAC TDC's were commonly cleared and started, and stopped in turn by successive pion signals, such that the first TDC held the first pion time, the second one the second pion time, etc. For SX(L) events pions were recorded in the interval [-7.85 μs, 7 μs] relative to the pion that led to the $\pi S4$ trigger, for XX events between -8.6 and 6.25 μs relative to the detection of the second x ray.

If the stop-light conditions mentioned in Sec. II C were fulfilled, the scintillation light analyzer generated a $\pi S4$ trigger with a 900-ns delay relative to the starting pion signal. Additional delays in the amplifiers, cables, the high-voltage (HV) pulser to trigger the Pockels cell, the Nd:YAG and dye-laser systems, and the light path resulted in a total time difference of 1.6 μs between the pion entrance time and the arrival of the laser light in the cavity.

A $\pi S4$ trigger in coincidence with a 1X or 1XL gate started a πS gate with a width of 8 μs, but for events without laser (SX events) this gate was suppressed during the first 1.5 μs. The coincidence of the πS gate with a detected x ray caused a computer interrupt. The $\pi S4$ signal (in coincidence with a 1X or 1XL gate) also cleared and started all TDC's. (Fast CAMAC scalers clocked at 100 MHz acted as TDC's.) These TDC's were stopped by the signals t_x, t_L, which had fixed delays relative to the "true" times to record also "negative" times.

The signals from the fast preamplifiers of the x-ray detectors (MWPC's) were first passed through the pulse-shape analyzers (PSA's), which tested the zero-crossing times of suitably delayed, inverted, and summed pulses [22]. For an XX event the coincidence XX of two x rays with a time difference less than 500 ns had to occur within an XX gate. For XX events all times were started by the second x ray.

The diode array of the laser spectrometer was read out by a FADC. The pulse shape of the cavity diode was read out by a 100-MHz FADC. In addition, the time when the laser pulse entered the cavity (t_L) was recorded. The pulses of the pion entrance detector and of a 1-kHz clock were counted between two computer interrupts by two CAMAC scalers; the actual pion rate could thus be calculated in the off-line analysis as quotients of those rates. Upon a computer interrupt, further data taking was suppressed by inhibit-flip-flops (not shown in Fig. 8), and all CAMAC scalers, TDC's, and FADC's were read out by a PDP11/40 computer and stored on magnetic tape. The pictures taken by the CCD camera were continuously displayed on a TV screen, allowing an independent, very sensitive control of the cavity alignment. Once an hour such a picture was stored on a flexible disk by a personal computer (PC) equipped with a video frame-grabber board.

III. 2S LIFETIME

The $(\mu\mathrm{He})_{2S}$ decay is determined by the following contributions:

$$\frac{1}{\tau_{2S}} \cong \frac{1}{\tau_\mu} + \lambda_{xx} + \lambda_Q \ , \tag{1}$$

τ_μ being the muon lifetime and $\lambda_{xx} = 1.18 \times 10^5$ s^{-1} [19] the two-photon decay rate. The quenching rate λ_Q results from collisions with neighboring atoms or molecules and depends on the partial pressures of the various gas constituents. In practice, only He (4100 Pa), N_2 (9 Pa), and H_2O ($\sim$0.04 Pa) have to be taken into account; hence the total quenching rate is $\lambda_Q = \lambda_Q^{He} + \lambda_a^{N_2} + \lambda_Q^{H_2O}$. (The contribution from other impurities can be neglected, because the cross sections for 2S quenching are given by long-range ion-dipole forces and are therefore an order of magnitude larger for H_2O than for other molecules.) The 2S quenching rates depend nonlinearly on the partial pressures because one of the underlying processes is the formation of molecular ions in three-body collisions [10,27]. Numerical values will be given in Sec. III D.

A. Analysis of XX events

The 2S lifetime τ_{2S} was measured during the laser experiment by detecting both x rays from the two-photon decay. The probability for this decay channel corresponded to the product $\lambda_{xx}\tau_{2S}$. The sum of the two x ray energies was equivalent to the $K\alpha$ energy (8.22 keV). The 2S lifetime could be deduced either from the time slope of delayed two-photon events, or from the time-integrated number of such events in comparison with the number of prompt μHe-L-K transitions. To get these numbers, additional conditions had to be imposed upon the data in the off-line analysis. For XX events, only x rays with a detection time difference of less than 120 ns were accepted. The time of the muon stop for the delayed two-photon transitions was not directly given (for prompt L-K transitions it is defined by the detection time of the x rays, since the cascade time is negligibly short [11]). The detection time of delayed x rays had therefore to be referred to the entrance time of the last detected pion ("pilast"). In order to separate clearly the two-photon decays from the prompt L-K transitions, the time difference t between x ray detection and the entrance time of the last detected pion t_{pilast} had to exceed the maximum muon slowing down time $t_{\max}$ (1.1 μs). The number of detected two-photon decays in a delayed time interval was determined by the corresponding spectrum of energy sums of XX events, after the fitted background had been subtracted. To optimize the signal-to-background ratio in this

energy spectrum, two additional conditions upon the stop light (the pulse train of the stop detector) were required.

(i) In order to suppress uncorrelated background the number of scintillation photons in the interval $[t_{\text{pilast}}+0.1\ \mu\text{s}, t_{\text{pilast}}+1.3\ \mu\text{s}]$ had to be ≥ 3.

(ii) In order to suppress muon stops with large slowing down times, the amount of scintillation light was limited to ≤ 5 photons in the interval $[t_{\text{pilast}}+1.1\ \mu\text{s}, t_{\text{pilast}}+2.1\ \mu\text{s}]$. (The He-$N_2$-scintillation light occurred with delays up to a few microseconds).

A minute analysis of the data shows that 60% of the stopping muons fulfilled these two requirements ("$S3S5$ condition"), whereas the background was reduced by a factor of 8. Note that the $\pi S4$ condition did not act upon XX events.

B. Mathematical description

There are a number of events where the measured pion entrance times and the stop-light train do not unambiguously determine which one of the pions is physically correlated to the formation of a $(\mu\text{He})_{2S}$ atom emitting delayed x rays. The determination of τ_{2S} is still possible since the expected time distribution of two-photon decay events fulfilling the $S3S5$ condition can be described by a mathematical model, which will be sketched here in broad outline (details are given in Ref. [22]). For this description one has to distinguish between two cases which cannot be separated experimentally.

(a) The pion correlated to the two-photon decay and pilast are identical. For $t > t_{\max} = 1.1\ \mu\text{s}$ and the $S3S5$ condition, 82% of the two-photon decay events belong to this group.

(b) The correlated pion precedes t_{pilast}, but the $S3S5$ condition in the above-mentioned intervals after t_{pilast} is still satisfied because the scintillation light of the stopping muon has an "afterglow" of a few microseconds.

Next, the distribution $F_{\text{stop}}(t)$ of slowing down times for muons fulfilling the $S3S5$ condition is extracted from the data. Together with the rate of the entrance detector $\lambda_\pi = 4.55\times 10^5\ \text{s}^{-1}$ (dead-time corrected), it is possible to deduce for $t > t_{\max}$ the probability $W_{\text{xx}}(t)$ that the two-photon decay happens at a time t relative to t_{pilast}:

$$W_{\text{xx}}(t) = W_s e^{-\lambda_\pi (t-t_0)} e^{-t/\tau_{2S}} \frac{1}{\tau_{2S}} \times \int_0^{t_{\max}} e^{t_s/\tau_{2S}} F_{\text{stop}}(t_s)\,dt_s [1 + A(\tau_{2S})] \ . \quad (2)$$

$W_s = 0.60$ corresponds to the mentioned $S3S5$ acceptance. The factor $e^{-\lambda_\pi (t-t_0)}$ describes the probability of having no further pion between t_{pilast} and the two x rays, whereby the dead time $t_0 = 200$ ns of the entrance detector is also considered. $A(\tau_{2S})$ corresponds to the relative contribution of two-photon decays of case (b), which slightly depends on τ_{2S}. In good approximation Eq. (2) can be simplified [22]:

$$W_{\text{xx}}(t) = W_s H^0_{\text{xx}} e^{\bar{t}_s/\tau_{2S}} \frac{1}{\tau_{2S}} e^{-(\lambda_\pi + 1/\tau_{2S})t} \ , \quad (3)$$

with $H^0_{\text{xx}} = 1.40 \pm 0.03$, and the average slowing down time (with $S3S5$ condition) $\bar{t}_s = 0.29\ \mu\text{s}$.

C. Determination of the 2S lifetime

Two methods lead to the determination of τ_{2S}.

(i) By measuring the number of coincident x rays with energy sum $E_{x_1} + E_{x_2} = 8.22$ keV in various delayed time intervals. From a fit of $W_{\text{xx}}(t)$ to the measured data, τ_{2S} results according to Eq. (3), whereby only the slope in time, not the absolute amplitude has to be considered.

(ii) A second method results from the comparison of the number of measured prompt L-K transitions with that of two-photon decays detected in one broad delayed interval.

The results of method (ii) are particularly useful for the analysis of SXL events (Sec. IV) as they permit the most accurate determination of the expected number of $2S$ states existing at the laser injection time. This method will therefore be discussed briefly. The measured number of prompt L-K transitions, N_{LK}, fulfilling the $S3S5$ condition is linked to the corresponding number of muon stops $N_{\mu\text{-stop}}$ [28] by

$$N_{LK} = N_{\mu\text{-stop}} W(K\alpha) \langle E(L \rightarrow 2P, K\alpha) \rangle \langle A_{LK} \rangle W_s \ . \quad (4)$$

$W(K\alpha) = 0.784 \pm 0.023$ is the probability per muon stop, measured at 4.1 kPa, that a $K\alpha$ x ray occurs [11]. (Note that each $K\alpha$ is preceded by an L x ray since nonradiative transitions are completely negligible at this density.) $\langle E(L \rightarrow 2P, K\alpha) \rangle$ is the detection efficiency of both x rays and $\langle A_{LK} \rangle$ is the average acceptance of L-K transitions in the on-line pulse-shape analysis of signals from the x-ray detectors. Long-time instabilities of this analysis caused an L x-ray acceptance considerably less than unity for part of the data. This effect was taken care of by fitting the relative x-ray intensity ratios on a run-by-run basis, and by normalizing the results to those of runs where the L acceptance as ≥ 0.97, which was the case after the analyzer had been readjusted and tested with sources. The acceptance of $K\alpha$ x rays never dropped below 0.99. The average acceptance was $\langle A_{LK} \rangle = 0.92 \pm 0.03$.

The expected number of two-photon transitions $N_{\text{xx}}(t_1, t_2)$ falling in the delayed interval $[t_1, t_2]$ and satisfying the $S3S5$ condition is, for $t_1 \geq t_{\max}$,

$$N_{\text{xx}}(t_1, t_2) = N_{\mu-\text{stop}} \epsilon_{2S} \lambda_{\text{xx}} \tau_{2S} \langle E(X_1, X_2) \rangle \langle A_{\text{xx}} \rangle \times \int_{t_1}^{t_2} W_{\text{xx}}(t)\,dt \ . \quad (5)$$

Here, $\epsilon_{2S} = (2.6 \pm 0.3)\%$ is the relative $2S$ population per muon stop which, at low densities, can be deduced unambiguously from the measured K-line intensity ratios [11]. The factor $\lambda_{\text{xx}} \tau_{2S}$ is the relative number of two-photon decays. By taking the ratio $N_{\text{xx}}(t_1, t_2)/N_{LK}$, the number

of the not directly measured muon stops cancels and only relative values for the detection efficiencies and acceptances are to be compared:

$$\frac{N_{xx}(t_1,t_2)}{N_{LK}}=\frac{\epsilon_{2S}}{W(K\alpha)}\frac{\langle E(X_1,X_2)\rangle}{\langle E(L\rightarrow 2P,K\alpha)\rangle}\frac{\langle A_{xx}\rangle}{\langle A_{LK}\rangle}$$
$$\times\lambda_{xx}H^0_{xx}e^{\bar{t}_s/\tau_{2S}}\int_{t_1}^{t_2}e^{-(\lambda_\pi+1/\tau_{2S})t}dt\ . \quad (6)$$

The ratio of detection efficiencies $\langle E(X_1,X_2)\rangle/\langle E(L\rightarrow 2P,K\alpha)\rangle$ was determined to a value 1.91 ± 0.10 by a Monte Carlo simulation. This value includes the angular correlation between the x rays from two-photon decays. Its relative error is moderate, since in the ratio the solid angle cancels and the compared energies are not very different. The ratio of the electronical acceptances was found to be $\langle A_{xx}\rangle/\langle A_{LK}\rangle=1.06\pm0.03$.

D. Results

Figure 9 shows a measured single-energy spectrum of prompt XX events. For the majority of the events, one of the detectors recorded a μHe-$K\alpha$ transition and the other an L transition. The detection of higher μHe-K lines was suppressed due to the XX coincidence condition. The fitted function shown in Fig. 9 is composed of the $L\alpha$ (1.52 keV), $L\beta$ (2.05 keV), $L(>\beta)$ (2.52 keV), $K\alpha$ (8.22 keV) lines of μHe, several K-fluorescence lines of the Cr-Ni steel used for the target vessel (5.4–7.4 keV), a xenon escape line at about 4 keV, and a continuous x-ray background multiplied by the detector efficiency. If events are selected with an x-ray energy less than 4 keV in one of the detectors, the energy spectrum of the other one is dominated by the $K\alpha$ line. The total number of such $K\alpha$ events from both detectors is the number of detected prompt L-K transitions $N_{LK}=(356\pm4)\times10^3$.

The spectrum of measured energy sums for delayed XX events in the interval between $t_1=1.125$ μs and $t_2=2.5$ μs is given in Fig. 10. An additional analysis of the events in the peak at 8.2 keV proved that their single

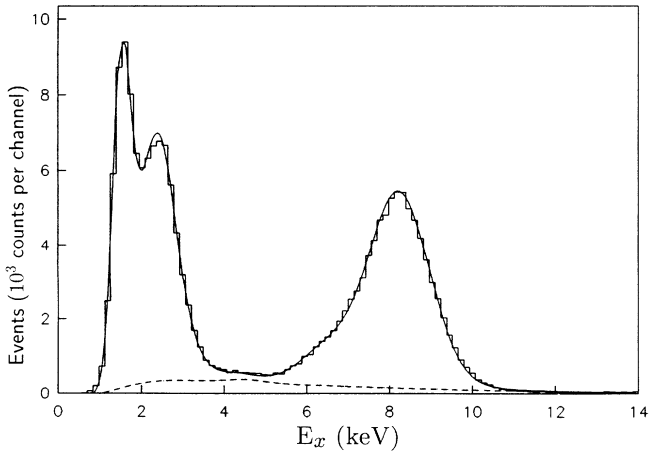

FIG. 9. Single energy spectrum of prompt XX events: The solid line corresponds to the fit described in Sec. III D, the dashed line to the continuous part of the background.

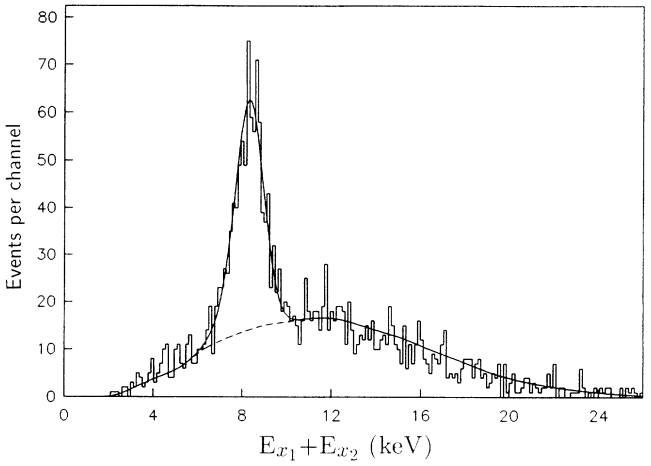

FIG. 10. Spectrum of energy sums $E_{X_1}+E_{X_2}$ of delayed XX events with $t_{xx}-t_{pilast}$ between $t_1=1.125$ μs and $t_2=2.5$ μs.

energies were distributed as expected for two-photon transitions [22]. The shown background function is the superposition of the background spectrum measured in each detector, which is essentially an energy continuum multiplied by the detection efficiency. The number of two-photon transitions in the peak is $N_{xx}(t_1,t_2)=623\pm45$, whereby the main uncertainty results from the uncertainty of the background. Inserting these numbers in (6) we get

$$\frac{\epsilon_{2S}}{W(K\alpha)}\lambda_{xx}e^{\bar{t}_s/\tau_{2S}}\int_{t_1}^{t_2}e^{-(\lambda_\pi+1/\tau_{2S})t}dt$$
$$=(6.14\pm0.59)\times10^{-4}\ , \quad (7)$$

and from this

$$\tau_{2S}=1.014\pm0.121\ \mu s\ . \quad (8)$$

The main contributions to the error given in (8) are the uncertainties of ϵ_{2S} and $N_{xx}(t_1,t_2)$.

To determine τ_{2S} by the first method (i), the number of two-photon events $N_{xx}(t_i,t_i+\Delta t)$ at various time intervals was fitted as for method (ii). From a fit of the exponential slope in time of these measured numbers (Fig. 11), $\tau_{2S}=1.016\pm0.136$ μs was deduced. The good agreement of both results shows the consistency between the two methods, which are quite independent. In particular, it corroborates the comparison of the absolute numbers of delayed and prompt events used for method (ii), which will be used analogously in the analysis of the laser events.

The quenching rates $\lambda_Q^{He}=(1.63\pm0.34)\times10^5\ s^{-1}$ and $\lambda_Q^{N_2}=(1.24\pm0.33)\times10^5\ s^{-1}$ (for 4.1 kPa He plus 0.22% N_2) were determined in earlier experiments [11,27]. The $2S$ quenching by H_2O was not measured; a rough estimation of the cross section (dominated by long-ranged ion-dipole forces) gives $\lambda_Q^{H_2O}=(0.8\pm0.5)\times10^5\ s^{-1}$ at a H_2O partial pressure of $(4\pm2)\times10^{-2}$ Pa. Inserting these values in (1) we obtain an expected $2S$ lifetime $\tau_{2S}=(1.06\pm0.08)$ μs, in good agreement with the directly measured value (8).

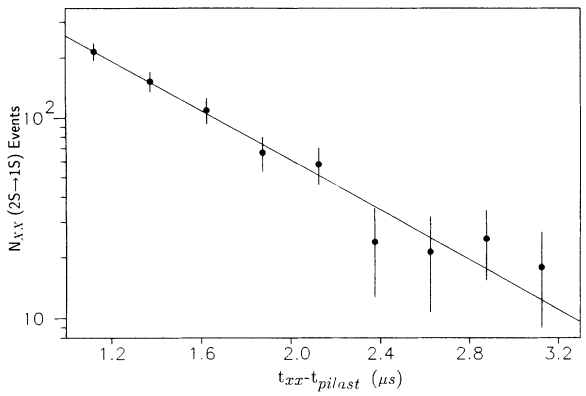

FIG. 11. Number of two-photon transitions $N_{xx}(t_i, t_i+\Delta t)$, determined from the corresponding spectra of energy sums measured for delayed intervals, with $\Delta t = 0.25$ μs.

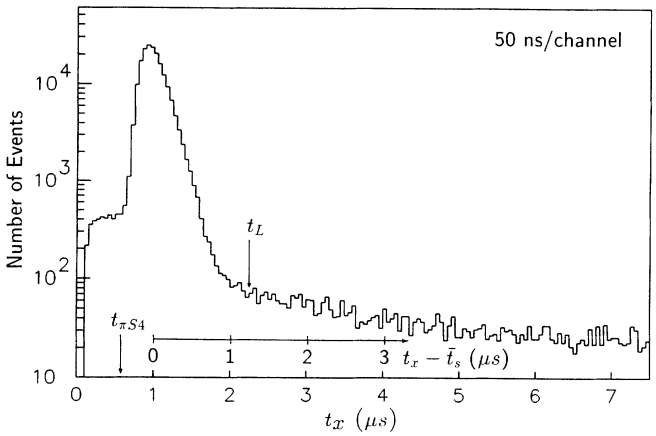

FIG. 12. Measured 8-keV time spectrum of SXL events (with laser) with x ray energies around $E_{K\alpha} = 8.22$ keV. The data from both detectors have been added up. The entrance time of the triggering pion is at $t_{\pi S4} = 0.61$ μs and the laser injection time at $t_L = 2.23$ μs. An additional scale illustrates the time differences relative to the mean muon stop time $\bar{t}_s$.

IV. LASER RESONANCE MEASUREMENT

A. Principle and data analysis

The goal of the experiment was to test the resonance wavelength $\lambda = 811.7$ nm of the $\mu^- {}^4\text{He}$ $2S_{1/2}$-$2P_{3/2}$ transition, found in the earlier experiment [3]. We searched for delayed $K\alpha$ x rays in coincidence with the laser pulse. If the wavelength is on resonance, an enhancement of the number of $K\alpha$ x rays with an energy around 8.22 keV should be observed in the time spectrum at the laser time.

In this spectrum (shown in Fig. 12) the time of the laser injection into the mirror cavity is at $t_L = 2.23$ μs, and the entrance time of the triggering pion is at $t_{\pi S4} = 0.61$ μs (the origin of the t axis was chosen arbitrarily). The laser is triggered with a fixed delay after a pion fulfilling the $\pi S4$ condition for the scintillation light ("stop light").

Qualitatively, the data shown in Fig. 12 give no evidence for a laser resonance. For a precise quantitative analysis, it is necessary to subtract the background from the data and to determine the number of remaining "laser-on" events, and to compare it to the calculated number of events expected on resonance. The latter can be deduced from (i) the number of prompt events in the time spectrum (Fig. 12), (ii) the probability that a $2S$ state is populated and survives until t_L, and (iii) the laser-induced $2S$-$2P$ transition probability. The values for (ii) and (iii) will be given in the following section. For the precise determination of (i), it was taken into account that the triggering pion is not always identical to the pion that produces the stopping muon. In 7.5% of the cases the laser trigger is started (incorrectly) by a pion which precedes or follows the correlated one. (The latter case explains the enhanced 8-keV x-ray rate at "negative" times $t_x < 0.61$ μs compared with late times.) The function of time correlations between the triggering and the correlated pion was calculated from an analysis of the detected scintillation light and the $\pi S4$ trigger electronics, and found to be in good agreement with measured data [22]. A detailed understanding of this correlation function guarantees that the correct value for (i) is extracted from the measured 8-keV time spectrum.

The time spectrum of x rays with energies around 8 keV without laser-induced transitions is composed of the following contributions.

(a) Prompt x rays from muon stops, correlated to the $\pi S4$ trigger. Their time distribution is mainly given by the stop-time distribution, increases sharply after $t_{\pi S4}$, and decreases nearly exponentially with $\tau \sim 100$ ns after the maximum. The energy distribution is dominated by the L and K lines of muonic helium, with a moderate contribution of steel fluorescence lines.

(b) Trigger-correlated x rays, which are produced by bremsstrahlung from the electron of the muon decay and thus, in the time spectrum, decrease exponentially with τ_μ. Their energy distribution is continuous.

(c) Trigger-correlated x rays, which are produced by μHe-$2S$ decays and decrease therefore exponentially with τ_{2S}. In particular, these are $K\alpha$ x rays from radiative $2S$ quenching or, less probably, single x rays from two-photon decays falling into the accepted 8-keV energy region.

(d) Time-independent ("flat") background of accidental x rays which are not correlated to the trigger. The energy distribution is mainly a continuum superposed by μHe L and K lines from muon stops not correlated with the trigger.

At the laser injection time the contributions (a)–(d) in the 8-keV time spectrum had to be considered as background, and therefore to be minimized in the on-line analysis by different cut conditions without strongly affecting possible laser-induced $K\alpha$ x rays. To reduce the contribution (a), a stop-light condition "CUT5" was used which rejected events with more than five scintillation

photons in the interval [1.0 μs, 1.6 μs] relative to the triggering pion and thus suppressed muon stops with long slowing down times. To "minimize" the contribution (b), an energy window $7.0 \leq E_x \leq 9.6$ keV was chosen, accepting most of the $K\alpha$ x rays (according to the detector energy resolution). The contribution (c) could not be reduced without suppressing laser-induced events proportionally. To minimize the flat background (d), a cut was defined which rejected events where a pion (not identical to the triggering pion) occurred within 0.5 μs before t_x ("π_{sd}cut").

From an analysis of the background at various times and energies, the relative contributions to the 8-keV time spectrum at t_L were determined to be 39% from (b), 32% from (c), and 28% from (d), whereas the contribution from muon stops (a) was negligible (1%), if the mentioned cuts were applied.

For the final analysis the small number of SXL events having a laser energy below 45 mJ was rejected. The data shown in Fig. 12 fulfill all these conditions.

B. 2*S*-2*P* transition probability

In order to deduce the expected number of laser-induced $K\alpha$ transitions, the mean 2*S*-2*P* transition probability has to be determined. On resonance, the 2*S*-2*P* transition rate $\lambda_{2S,2P}$ of a μHe ion in an external electromagnetic field with intensity I and polarization parallel to the z axis is [29]

$$\lambda_{2S,2P}=\frac{8\pi\alpha I Z_r^2}{\Gamma\hbar}|\langle 2P|\mathbf{Z}|2S\rangle|^2=Kf_{2S,2P}I \ , \tag{9}$$

with the recoil correction for the "effective radiative charge" $Z_r=1+(Z-1)m_\mu/(m_{\mathrm{He}}+m_\mu)=1.03$ [19], $\Gamma=\tau_{2S}^{-1}+\tau_{2P}^{-1}=2\times10^{12}$ s^{-1}, and $K=1.44$ J^{-1} cm^2. The value of the Clebsch-Gordan coefficient $f_{2S,2P}$ is $\frac{1}{3}$ for the transition to the $2P_{1/2}$ state and $\frac{2}{3}$ for the transition to the $2P_{3/2}$ state. The total probability $\omega_{2S,2P}(t)$ that a 2*S* state existing at $t=0$ undergoes a transition during the time interval $[0,t]$ obeys the differential equation

$$\frac{d\omega_{2S,2P}(t)}{dt}=e^{-t/\tau_{2S}}[1-\omega_{2S,2P}(t)]\lambda_{2S,2P} \ . \tag{10}$$

In the case of a constant laser intensity I in $[0,T]$ the total 2*S*-2*P* transition probability is

$$\begin{aligned}\omega_{2S,2P}&=\omega_{2S,2P}(T)\\&=1-\exp[-Kf_{2S,2P}I\tau_{2S}(1-e^{-T/\tau_{2S}})] \ .\end{aligned} \tag{11}$$

In practice (10) was integrated numerically, using the measured intensity distribution $I(t)$ (cf. Fig. 7), but the deviations from (11) were small ($<2\%$). The approximation (11) will therefore be used henceforth.

The spatial intensity distribution within the four-mirror cavity is not uniform. A local transition probability has therefore to be defined, and the mean transition probability can be determined by integration over the muon-stop volume. Detailed computer simulations showed that the space-time correlation of the intensity distribution can be neglected in good approximation, since, for geometrical reasons, every place crossed by the laser pulse at the time $\hat{t}$ will be hit a second time by the laser pulse at $T-\hat{t}$. In addition, the decrease in intensity, caused by reflection losses, is small [$(14\pm8)\%$ after $N=30$ round trips]. The local distribution of the time-integrated intensity ("energy per area") in the cavity was deduced from the information of the CCD camera. The calibration of this energy distribution was obtained from the pulse shape of the cavity diode by equalizing the space integral of the local energy distribution to the measured and calibrated time integral of the diode. The pulse shape of the diode was recorded for each laser event, whereas a representative CCD picture was stored about once an hour. The justification for this procedure was that simulations demonstrated that the 2*S*-2*P* transition probability was quite insensitive to small displacements of the laser beam, whereas it depended almost proportionally on the diode integral, which fluctuated up to 10% from event to event.

For each event, the laser energy distribution per unit area $F(x,y,z)$ was deduced from the data as described above. Together with the muon-stop distribution $\rho_{st}(x,y,z)$, calculated by a Monte Carlo simulation of the muon bottle, the local transition probability $\omega_{2S,2P}(x,y,z)$ and the mean transition probability $\varepsilon_{\mathrm{laser}}$ could be determined:

$$\begin{aligned}&\omega_{2S,2P}(x,y,z)=1-e^{-Kf_{2S,2P}F(x,y,z)f_{\mathrm{red}}} \ ,\\&\varepsilon_{\mathrm{laser}}=\int_{\text{stop vol}}\omega_{2S,2P}(x,y,z)\rho_{st}(x,y,z)dV \ .\end{aligned} \tag{12}$$

$f_{\mathrm{red}}=\tau_{2S}(1-e^{-T/\tau_{2S}})/T$ describes the reduction of the transition probability resulting from the 2*S* decay during the illumination of the cavity. By averaging over all accepted laser events we deduced a mean transition probability $\langle\varepsilon_{\mathrm{laser}}\rangle=0.055\pm0.005$, where the uncertainty resulted mainly from the energy monitoring (cf. Sec. II G) and from the not precisely known position of the muon-stop distribution relative to the laser energy distribution ($\pm5\%$ contribution to $\Delta\varepsilon_{\mathrm{laser}}/\varepsilon_{\mathrm{laser}}$).

The laser-induced 2*P* state was polarized ($l_z=0$) corresponding to the laser polarization. Hence the probability of emitting a $K\alpha$ x ray (immediately following the 2*S*-2*P* transition) was proportional to $\sin^2\vartheta$, ϑ being the angle between the laser polarization and the direction of emission. The laser light was polarized in the z direction defined in Fig. 2. As a consequence the two x-ray detectors had different detection probabilities. The ratio of the detection probabilities for laser-induced $K\alpha$ from polarized 2*P* states and the one from unpolarized 2*P* states (uniformly distributed $K\alpha$), $f_{\mathrm{pol}}^{\gamma}(\gamma=y,z)$, was calculated for each detector by integrating over the muon-stop distribution: $f_{\mathrm{pol}}^{y}=1.37\pm0.03$ for detector y, and $f_{\mathrm{pol}}^{z}=0.37\pm0.01$ for detector z.

C. Results and conclusions

With the number of prompt $K\alpha$ x rays $(N_{K\alpha}^{p})_\gamma$ measured in each detector ($\gamma=y,z$), it is possible to determine the number of laser-induced $K\alpha$ x rays expected on resonance:

$$(N_{K\alpha}^{\text{laser}})_\gamma = (N_{K\alpha}^{p})_\gamma \frac{\epsilon_{2S}}{W(K\alpha)} \times e^{-(\bar{t}_{\text{ST-}L}/\tau_{2S})} A_{\text{cut}} f_{\text{pol}}^{\gamma} \langle \varepsilon_{\text{laser}} \rangle a_t \ . \quad (13)$$

$\bar{t}_{\text{ST-}L} = 1.23$ μs is the mean time difference between muon stop and laser injection in the cavity corresponding to a mean slowing down time of 0.39 μs. $A_{\text{cut}} = 0.883 \pm 0.004$ is the relative acceptance ratio "delayed relative to prompt" of the π_{sd} cut. The expected time distribution of laser-induced events is given by the cavity entrance time $t_L = 2.23$ μs and the convolution of the measured functions of light intensity (Fig. 7), with the x-ray detector resolution (Fig. 3). It turns out that a fraction $a_t = 0.95$ of all laser-induced events is expected within the time interval [2.25 μs, 2.55 μs]. The comparison of expected and measured number of events will henceforth be restricted to this interval.

The numbers of prompt events $(N_{K\alpha}^{p})_\gamma$ were deduced from a fit of the 8-keV time spectra of SXL events, which were selected as described in Sec. IV A. A small background from admixtures of μHe-$K\beta$ and steel-fluorescence lines was subtracted. The resulting numbers are $(N_{K\alpha}^{p})_y = (8.9 \pm 0.1) \times 10^4$ and $(N_{K\alpha}^{p})_z = (9.2 \pm 0.1) \times 10^4$. The numbers $(N_{K\alpha}^{\text{laser}})_\gamma$ for laser-induced events expected on resonance, given in Table I, were calculated from Eq. (13). Their relative uncertainty of 14% resulted mainly from the uncertainty of $\langle \varepsilon_{\text{laser}} \rangle$ (10%) and the uncertainty of the probability to have a 2S state at the time the laser was injected into the cavity. Based on the results from the analysis of XX events [Eq. (7)], the relative uncertainty of the term $[\epsilon_{2S}/W(K\alpha)]e^{-(\bar{t}_{\text{ST-}L}/\tau_{2S})}$ can be limited to 10%, since $\bar{t}_{\text{ST-}L}$ is close to the center of gravity of $W_{xx}(t)$ in the interval $0.84 \le t - \bar{t}_s \le 2.21$ μs, in which the number of two-photon decays was measured.

For the determination of the measured number of laser-induced $K\alpha$ x rays we compared the delayed regions of the 8-keV time spectra of SXL events (with laser) and of SX events (without laser). For each detector the much more populated time spectrum of SX events was normalized to the SXL spectrum in the delayed interval [2.6 μs, 7.5 μs], which did not include the interval in which the laser events were expected. The relative error of the normalization factors is mainly given by the number of SXL events in this interval (approximately 1800 per detector) and amounts to $[(1800)^{-1} + (16000)^{-1}]^{1/2} = 2.5\%$. For each detector the normalized SX spectrum was then subtracted channel by channel from the SXL time spectrum. The sum of the two resulting background-free difference spectra from the two detectors is shown in Fig. 13. While statistical variations are present, no resonance effect is discernible.

The number of events measured in the time interval [$t_1 = 2.25$ μs, $t_2 = 2.55$ μs] for SXL events, $N_{8\text{ keV}}^{\text{meas}}$, is given in Table I, together with the number of background events without laser, $N_{\text{bg}[t_1,t_2]}$, which is the number of measured SX events multiplied by the normalization factor. The difference between the two numbers is the number of measured laser-induced $K\alpha$ x rays, which is for both detectors compatible with zero and in disagreement with the number $N_{K\alpha}^{\text{laser}}$ expected on resonance.

For the analysis of the compatibility of the measured with the expected numbers, we calculated the probability that the measured numbers belong to the statistical distributions to be expected on resonance. The expected number of events, including background, is Poisson-distributed around the mean value $\mu = N_{K\alpha}^{\text{laser}} + N_{\text{bg}[t_1,t_2]}$, which is the sum of expected laser events and measured background. The resulting values for μ and its uncertainties $\Delta\mu$ are given in Table I. In practice, the Poisson distribution may be replaced by a Gaussian, and its width $\mu^{1/2}$ can be quadratically added to the uncertainty of the mean value: $\sigma_{\text{tot}} = (\mu + \Delta\mu^2)^{1/2}$. The measured value corresponding to this distribution is $N_{8\text{ keV}}^{\text{meas}}$. The differences $\mu - N_{8\text{ keV}}^{\text{meas}}$ (Table I) were divided by the Gaussian width

TABLE I. Measured and expected number of 8-keV x rays in the delayed interval [2.25 μs, 2.55 μs], where laser-induced $K\alpha$ x rays are expected, for both detectors.

	Description	Detector y	Detector z	Detector $y+z$
Measured:	With laser (includes bg[a]): $N_{8\text{ keV}}^{\text{meas}}$	211±14.5	199±14.1	410±20.2
	Without laser (bg[a] normalized): $N_{\text{bg}[t_1,t_2]}$	209±7.1	222±7.5	431±10.3
	Difference	2±16.1	−23±16	−21±22.7
Expected:	$N_{K\alpha}^{\text{laser}}$ (on laser resonance)	58±8.3	16±2.3	74±10.6
	$\mu = N_{K\alpha}^{\text{laser}} + N_{\text{bg}[t_1,t_2]}(\pm\Delta\mu)$	267±10.9	238±7.8	505±14.8
Compatibility:	$\mu - N_{8\text{ keV}}^{\text{meas}}(\pm\sigma_{\text{tot}})$	56±19.6	39±17.3	95±26.9
	Deviation in σ terms	$2.86\sigma_{\text{tot}}^{y}$	$2.25\sigma_{\text{tot}}^{z}$	$3.53\sigma_{\text{tot}}$
	W_{res}	4.3×10^{-3}	2.4×10^{-2}	4.3×10^{-4}
	$W_{\text{off-res}}$	0.901	0.151	0.355
	$\alpha = \frac{W_{\text{res}}^{y}}{W_{\text{off-res}}^{y}} \frac{W_{\text{res}}^{z}}{W_{\text{off-res}}}$		7.6×10^{-4}	1.2×10^{-3}

[a]bg denotes background.

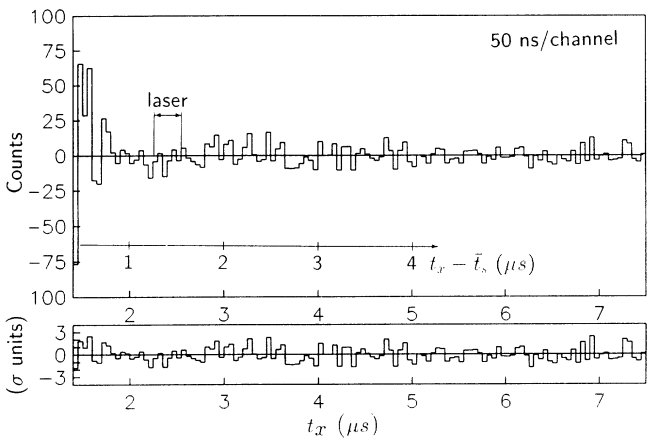

FIG. 13. Difference spectrum resulting from a channel-by-channel subtraction of the normalized 8-keV time spectrum of SX events (without laser) from the 8-keV time spectrum of SXL events (with laser). On resonance, laser-induced events are expected in the indicated time interval between 2.25 and 2.55 μs. In the lower spectrum the differences are given in units of standard deviations (σ) by dividing the content of each channel of the upper spectrum by its statistical error (including the normalization error).

σ_{tot} to determine the probability W_{res} that the measurements are compatible with the values expected on resonance. The deviation is 3.5σ for the combined result of both detectors. The same procedure was performed for the assumption that the laser was off resonance. The resulting level of significance $\alpha = W_{\text{res}}/W_{\text{off-res}}$ is 5×10^{-3} for detector y alone and less than 2×10^{-3} for both detectors combined.

The tested wavelength $\lambda = 811.7$ nm (value measured in air, as in Ref. [3]) is excluded by these data, with the level of significance given above. Moreover, by taking into account the natural linewidth $\Delta\lambda = \Gamma\lambda^2/(2\pi c) = 0.7$ nm of the $2S$-$2P$ transition, the wavelength region $811.4 \le \lambda_{2S\text{-}2P} \le 812.0$ nm can be rejected as resonance wavelength with a confidence level greater than 95%.

In an attempt to explain the long $2S$ lifetime found in some of the high-pressure experiments, it has been suggested in Ref. [15] that excited molecular ions $\{\text{He-}(\mu\text{He})^+_{2S}\}^{*+}$ are formed at high gas densities. However, the corresponding correction of the $2S$-$2P$ resonance wavelength due to the screening by the molecular electrons was calculated to be only $\Delta\lambda = 0.13$ nm [30]. The discrepancy between the results of the earlier experiment and the present laser experiment can therefore not be resolved by the existence of molecular ions. The determination of the $2S$-$2P$ energy difference in μHe must be left to future experiments at low densities, where molecular effects are negligible. A wavelength range from 809 to 815 nm will have to be scanned according to the value of 812.2 ± 1.5 nm predicted by QED calculations and electron scattering data.

ACKNOWLEDGMENTS

We thank L. M. Simons for his help during the measurements. R. Kramer made the software and parts of the hardware of the CCD camera read-out system. C. Brandes, F. Dittus, P. Egelhof, and H. Heeb participated significantly in various stages of the experiment. The experiment benefited from various discussions with E. Zavattini and D. Taqqu. Excellent technical support was provided by R. Leuenberger, B. Schultheiss, G. Wemmers, and many members of the PSI technical staff. The intricate power supply and high-voltage devices of the laser system were engineered by M. Horvat and G. Irminger. This project was supported by the Paul Scherrer Institute.

*Present address: Optiray AG, CH-6330 Cham, Switzerland.
†Present address: ESEC SA, CH-6330 Cham, Switzerland.
‡Present address: General Electric Company, Schenectady, NY 12301.

[1] E. Zavattni, in *Exotic Atoms,* edited by G. Fiorentini and G. Torelli (Servizio Documentazione dei Laboratori Nazionali di Frascati, 1977), p. 43.
[2] E. Borie and G. A. Rinker, Phys. Rev. A **18**, 324 (1978); Rev. Mod. Phys. **54**, 67 (1982).
[3] G. Carboni *et al.*, Nucl. Phys. **A278**, 381 (1977).
[4] G. Carboni *et al.*, Phys. Lett. **73B**, 229 (1978).
[5] A. Placci *et al.*, Nuovo Cimento **1A**, 445 (1971).
[6] A. Bertin *et al.*, Nuovo Cimento **26B**, 433 (1975).
[7] R. O. Müller *et al.*, Phys. Rev. A **11**, 1175 (1975).
[8] G. Carboni and O. Pitzurra, Nuovo Cimento **25B**, 377 (1975).
[9] J. S. Cohen and J. N. Bardsley, Phys. Rev. A **23**, 46 (1981).
[10] H. P. von Arb *et al.*, Phys. Lett. **136B**, 232 (1984).
[11] F. Dittus, Ph.D. thesis, Eidgenössische Technische Hochschule Zürich, 1985 (unpublished).
[12] J. S. Cohen, Phys. Rev. A **25**, 1791 (1982).
[13] D. P. Grechukhin *et al.*, Zh. Eksp. Teor. Fiz. **91**, 1598 (1986) [Sov. Phys. JETP **64**, 942 (1987)].
[14] J. Menshikov *et al.*, Z. Phys. D **7**, 203 (1987).
[15] L. Bracci and E. Zavattini, Phys. Rev. A **41**, 2352 (1990).
[16] M. Eckhause *et al.*, Phys. Rev. A **33**, 1743 (1986).
[17] H. Orth, in *Electromagnetic Cascade and Chemistry of Exotic Atoms,* edited by L. Simons *et al.* (Plenum, New York, 1990), p. 155.
[18] I. Sick, Phys. Lett. **116B**, 212 (1982).
[19] R. Bacher, Z. Phys. A **315**, 135 (1984).
[20] H. Anderhub *et al.*, Phys. Lett. **101B**, 151 (1981).
[21] J. Deutsch *et al.*, SIN Newsl. **17**, 26 (1984).
[22] P. Hauser, Ph.D. thesis, Eidgenössische Technische Hochschule Zürich, 1991 (unpublished).
[23] Ch. Lüchinger, Ph.D. thesis, Eidgenössische Technische Hochschule Zürich, 1990 (unpublished).

[24] Ch. Lüchinger *et al.*, Opt. Eng. (to be published).
[25] D. J. Brink and C. J. van der Hoeven, Rev. Sci. Instrum. **55**, 1948 (1984).
[26] A. Biancchetti *et al.*, PSI Nucl. Part. Phys. Newsl. **1989**, 67 (1989).
[27] F. Dittus *et al.* (unpublished).
[28] The number of muon stops, $N_{\mu\text{-stop}}$, is restricted to muons reaching the μHe $1S$ or $2S$ state. One cannot exclude the fact that approximately 1% of the stopped muons form metastable μHe systems in highly excited states. Such muons are treated in the analysis like muons decaying before being stopped. The formation of metastable states in exotic He atoms has long been known as "Condo's hypothesis" and has recently been confirmed experimentally for kaonic and antiprotonic helium [M. Iwasaki *et al.*, Phys. Rev. Lett. **67**, 1246 (1991)].
[29] E. Merzbacher, *Quantum Mechanics* (Wiley, New York, 1970).
[30] L. Bracci, A. Vacchi, and E. Zavattini, Laboratori Nazionali di Frascati Report No. INFN/AE-91/07, 1991 (unpublished).